The role of particle sinks and sources in Alcator C-Mod detached divertor discharges

B. Lipschultz, J.L. Terry, C. Boswell, J.A. Goetz, A.E. Hubbard, S.I. Krasheninnikov, B. LaBombard, D.A. Pappas, C.S. Pitcher, F. Wising* and S. Wukitch

Massachusetts Institute of Technology, Plasma Science & Fusion Center, Cambridge MA. 02139

Abstract

Detailed measurements of the magnitude and location of volumetric recombination occurring in the detached divertor of Alcator C-Mod tokamak [I.H. Hutchinson *et al.*, Phys. Plasmas **1**, 1511 (1994)] are presented. The drop in divertor plate ion current during detachment is due to two mechanisms: (1) volumetric recombination in the divertor plasma; and (2) reductions in the divertor ion source. Depending on plasma conditions, each of these can be the primary mechanism for the observed ion current reduction in detachment. The ion source during detachment is inferred and its magnitude is consistent with the measured divertor power flow. A scaling of the density in the divertor recombining region for L- (Low confinement) mode plasmas is found, $n_{e,r} \propto \bar{n}_e^{0.8} \cdot P_{SOL}^{2/7}$. A model based on pressure variation along a flux surface during detachment is consistent with the main features of this scaling.

* current address Ericsson Microwave Systems AB, SE-431 84 Mölndal Sweden

PACS numbers: 52.55.Fa, 34.80.Lx, 52.25.Qt, 52.25.Rv

I. INTRODUCTION

The general experimental features of divertor detachment have been fairly well characterized (*e.g.* Ref. 1-5). Most important among these are reductions in plasma pressure and heat flux at the divertor plate relative to attached (or upstream) values. These are accompanied by a reduction in ion flux at the plate. These essential features explain the attraction of this mode of operation because the highly concentrated power flowing along flux tubes towards the divertor plate is dissipated, through radiation and neutral transport. The concentrated power flowing to a small region of the divertor plate is thus dispersed over much larger regions of the first-wall. This is very beneficial for optimizing tokamak operation, or any magnetically-confined plasma operation, in that reduced power and particle fluxes to the divertor plates reduces erosion and impurity sources, increases component lifetime and margins of safety.

The conditions that can lead to detachment include low temperatures ($T_e \leq 5$ eV) in the divertor region[6,7]. During detachment, T_e can reach very low values (~ 1 eV)[8-9]. Modeling has also shown that volume recombination should be significant in such low temperature detached divertor plasmas and potentially provide the mechanism for the observed divertor plate current reduction[10-14]. Recombination has been experimentally shown to exist in the divertor[15-24] and its magnitude to be significant[15,17,19,21,22,24] in comparison to the ion current reduction to the divertor plates. Measurements made on linear devices lead to similar conclusions[25,26]. More detailed measurements are still needed to understand the magnitude and location of recombination over a wide range of conditions. This will determine if recombination is an important part of detachment or merely a byproduct of the low temperatures. Such measurements will also provide divertor models with stringent tests of the atomic physics included therein.

In this paper we present detailed measurements of the recombination magnitude and location in the Alcator C-Mod tokamak divertor region. The recombination ion sink can dominate the observed reduction in ion flow to the divertor plates. We infer that an equally important mechanism for plate ion current reduction is the reduction in the ion source rate further upstream in the divertor. Limitations or reductions in the power flow into the ionizing region appear to be the cause of the inferred ion source changes.

II. EXPERIMENT AND TECHNIQUE

The measurements presented here are from the Alcator C-Mod tokamak. Basic characteristics of the experiment and diagnostics are described elsewhere[27]. The data used in this study were acquired with 5.3 Tesla toroidal field at the plasma center and plasma currents in the range 0.8-1.0 MA. All discharges were diverted with a single field null at the bottom of the machine, Fig. 1. Included in this study are data from Ohmically-heated as well as ICRF-heated (Ion Cyclotron

Radio-Frequency-heated) discharges. The heated discharges include both L- (Low-confinement) and H- (High confinement) modes. The H-mode discharges are described as Enhanced D-alpha (EDA) H-modes[28,29]. This relatively new enhanced confinement regime has confinement properties similar to ELM (Edge Localized Modes)-free and Type-1 ELMy H-modes but without the negative characteristics of impurity accumulation and bursts of high-power impacting the divertor plates respectively.

The primary diagnostics used for this study were visible and VUV (Vacuum UltraViolet) spectrometers, a CCD (Charge-Coupled Device) camera, and Langmuir probes located on the surface of the divertor plates. The visible spectrometer has an instrumental resolution of ~0.2 nm and a spectral range of 200 - 1300 nm. It is used to simultaneously monitor 16 inputs, each corresponding to a different chord within the views 'O' and 'T' of the plasma, Fig. 1. The second spectrometer, a vacuum instrument, is used to study the VUV spectrum around the Lyman series limit (instrumental resolution ~0.1 nm). It has a single, nearly horizontal viewing chord, that can be scanned to look through the x-point and above. The spectral range of the VUV spectrometer is 10-160 nm. The CCD camera has a tangential view of the divertor region and is filtered to image only D_γ light. Such images can be analyzed to obtain the local D_γ emissivity. A geometry matrix which connects the individual camera pixel brightnesses with the emissivities along the line of sight is generated and is then inverted using a singular value decomposition method for a given camera viewing orientation[30]. The emissivity profile is obtained from each CCD image by matrix multiplication of the inverted geometry matrix with the pixel brightness vector. The Langmuir probes are described in detail elsewhere[8].

Volume recombination of ions into neutrals can occur through several paths: radiative recombination, three-body recombination, and Molecular-Activated Recombination[19,26,31-34]. To date the latter has not been shown to be an important process in comparison to the three-body recombination in tokamak plasmas and has been extremely difficult to diagnose there[19]. The method used for the current study to estimate the volume recombination rate provides the sum total of radiative and three-body rates. It is based on previous work in which a collisional radiative model has been used to interpret the measured D^0 intensities (Ref. 19 and references therein). A factor R, 'recombinations per photon', is defined and calculated, which allows determination of the recombination rate, given knowledge of the emitting region density (n_e), temperature (T_e), a D^0 line brightness, and opacity of the plasma to the Lyman series emission, especially Ly_α[19]. We have not included the effects of radiation transport in wavelength and space which is the subject of another study[21]. We have applied this formalism to the spatially resolved D_γ brightnesses using the n_e and T_e, inferred from spectra obtained along the same viewing chord along with an estimated plasma opacity.

We have analyzed Lyman and Balmer series spectral brightnesses to determine the characteristics of the divertor plasma, Fig. 2(a,b). *Such characteristics are an average over the viewing chord, strongly weighted towards the highest emissivity regions*. The primary characteristic of both Balmer and Lyman spectra is that the line intensities $I_{p \rightarrow q}$ are produced by upper state population resulting from recombination, as evidenced by the fact that those intensities decrease much more slowly for increasing p than in the case where the emission is produced by excitation from the ground state[19,21]. The higher-p Balmer lines in such a spectrum are also significantly broadened compared to the instrumental width. We have fit a Voigt profile to these line shapes. Subtracting the contributions due to Doppler, instrumental and Zeeman effects, we then obtain the Lorentzian FWHMs (Full Width Half Maximum) of the $p=6,7,8,9 \rightarrow 2$ lines. Data and fit for a $p=8 \rightarrow 2$ line are shown in Fig. 2(c). Using standard Stark analysis techniques (*e.g.* Ref. 35), we obtain the density from any one transition emission line with an uncertainty of 2-3x$10^{20}$$m^{-3}$. Agreement of the density extracted from each of the $6,7,8 \rightarrow 2$ lines is typically within 10%, better than the uncertainty of fitting an individual line.

We have estimated the electron temperature from such a recombination-dominated Balmer spectrum. In these regimes the population density for each level should scale according to the Saha-Boltzmann distribution. We fit the population densities to that distribution:

$$n_p \quad \frac{p^2}{T_e^{3/2}} \exp\left(\frac{13.605}{T_e p^2}\right) \qquad (1)$$

where $(13.605/p^2)$ is the ionization energy for the pth level. In practice we perform a least-squares fit to a set of line ratios, n_p/n_q (*e.g.* p=5, q=6-8). Using such ratios makes the analysis simpler because the $T_e^{3/2}$ term in Eq. 1 is eliminated. An example of the result of such an analysis is given in Fig. 2(d). Due to the overlap of the $p = 9 \& 10 \rightarrow 2$ lines as well as their large 'wings', which are difficult to fit, we have only included the p=5 through $8 \rightarrow 2$ lines in this T_e analysis. The inferred electron temperatures are found to be in the range from 0.4 to 0.8 eV. The uncertainty of these temperatures is estimated (described later) to be ≤ 0.2 eV

As an independent confirmation of the density and temperatures determined above we have modeled the VUV spectrum near the Lyman series limit, Fig. 2(a). The continuum intensity for λ ≤ 91 nm is dominated by free-bound radiative recombination and is $n_e^2 \Delta L e^{-h\nu/kT}$, where ΔL is the characteristic radial width of the emission region and is determined through CCD camera imaging of the divertor. A sample fit is shown in Fig. 2(a). n_e (T_e) is determined from the intensity (slope) of the spectrum. The uncertainty in the fit is typically ≤ 0.1 eV. In the few cases where the views of the VUV and visible spectrometers coincide, the n_e and T_e derived from the two spectra

agree to within experimental uncertainties. Since the visible spectrometer has many chords spanning the divertor region, we relied on that instrument for most of the data presented herein.

Although the Balmer T_e technique outlined above is more easily applied at many points in the divertor, it is more uncertain. The uncertainties introduced by the fit to the Balmer population densities is typically small (< 0.1 eV). However, an additional uncertainty is added by the assumption that all the population densities used in this fit are completely determined by recombination, as opposed to excitation from the ground state. In a previous study of similar discharges[15] we used D_α intensities to estimate that the excitation contribution to the p=3 state to be approximately 30% of that from recombination. Assuming a larger excitation contribution (= recombination) to p=3 to allow for varying discharges and views, we utilize the collisional radiative model described earlier to predict the excitation contribution to the higher p states used in this Balmer T_e analysis. This effect leads to poorer fits to the data and an increase in T_e of ~ 0.1 eV. An uncertainty is also introduced by the opacity of the plasma to $Ly_{\alpha,\beta}$ which can lead to changing of the population densities. This is more difficult to estimate. However, since the Lyman continuum derivation of T_e is not subject to these uncertainties, we have conducted a comparison of temperatures obtained from the Balmer- and Lyman-continuum-based techniques[36]. Through this analysis we estimate the overall uncertainty in the Balmer-series estimate of T_e to be ~ 0.2 eV.

In the density and temperature range of interest (n_e ~1-2x$10^{21}m^{-3}$, T_e ~ 0.4-1.0 eV), the local recombination rate, S_R, which is proportional to the photon emission rate, is a strong function of n_e and T_e - $S_R \sim (n_e/T_e)^3$ (See reference 37 for an example of recombination rates and their dependence on plasma characteristics). Thus the recombining region n_e and T_e inferred from the spectrum of each viewing chord are characteristic of the strongest recombination emission region along the viewing path[38]. As described above, we can then determine the proportionality between the $D^0(p \rightarrow 2)$ line brightness and the recombination rate integrated along that chord given the assumed plasma opacity.

If the viewed plasma is opaque to Lyman series radiation, the local recombination and ionization rates are strongly affected. By measuring Ly_β and D_α intensities along the same line-of-sight through a recombining region, we have found[19] that up to 50% of the Ly_β photons are trapped and lost before reaching the spectrometer. This implies even stronger trapping (≥95%) of Ly_α emission. The modeling of the effect of such $Ly_{\alpha,\beta}$ trapping on the recombination rate shows that in these plasmas, trapping reduces the recombination rate by a factor of 2-5, depending on the local T_e, relative to the optically-thin case[19]. Because the VUV spectrometer used for the characterization of plasma opacity is not available at all times and has a limited set of views, we have assumed that the plasma opacity is the same in all divertor recombination regions. This assumption may potentially lead to underestimates of the recombination rates by a factor of ≤ 2.

III. RESULTS

A. Expansion of the recombination region

The location of the volume recombination region is important for understanding its development and its effects on the plasma. The initial growth of the recombination region at the outer divertor plate as detachment starts is shown in Fig. 3 (a-c) for a 1 MA Ohmic discharge where $\bar{n}_e$ is increased from $1.5 \times 10^{20} m^{-3}$ at 0.4 seconds to $3.3 \times 10^{20} m^{-3}$ at 0.95 seconds. These data are derived from viewing chords within view 'O', shown in Fig. 1, where the viewing chords are almost perpendicular to the plate surface. Each chord provides information about the plasma characteristics from the dominant D^0 emission region along the viewing chord which intersects the plate at a particular height z above the strike point (z=0). For reference, the outer divertor 'nose' (see Fig. 1) is at z ~ 5 cm. Divertor detachment, identified as a localized pressure loss occurring between the plate and upstream, starts at ~ 0.6 seconds in the vicinity of the separatrix and spreads across the viewing region until ~ 0.8 seconds, when the entire plate region in view 'O' is detached (as determined from pressure loss at the plate). Even in the initial time frame shown (0.55 s), before any observable pressure loss in the divertor, there is a high n_e (3a), low T_e (3b), recombining region (3c) across the field of view. Because the electron temperatures measured by probes along the divertor plate are much higher at this time (~5-10 eV in common flux region, 2-5 eV in the private flux region), we postulate that the high densities and low temperatures determined from analysis of the Balmer spectrum at 0.55 sec. are most likely from the private flux region. Such measurements have been reported previously[22,39]. As $\bar{n}_e$ is increased, the maximum in the measured density profile increases and the high density region expands up the plate. The T_e profile of Fig. 3(b) stays fairly constant while T_e derived from Langmuir probes in detached regions on the divertor surface drops to 1-2 eV. The corresponding recombination rate, determined from the D_γ brightnesses and the formalism discussed in Section II, also increases and the recombining region expands up the plate, Fig. 3(c). The profile at the last time shown is such that a significant amount of recombination is beyond this set of spectrometer views (view 'O') and was primarily monitored by the view from the top of the machine (view 'T', Fig. 1).

More information about the recombination region shape and expansion is found in the D_γ emissivity contours obtained from the CCD camera. An example of such an image for the same discharge as Fig. 3 is shown in Fig. 4. Soon after detachment begins ($\bar{n}_e = 2.3 \times 10^{20} m^{-3}$) the recombination is concentrated near the outer divertor plate, Fig. 4a. (We note that the 1 cm spatial resolution of the inferred emissivity profile is not sufficient to definitively determine whether all, or part, of the observed emission is from the private flux region.) As the density is increased to $\bar{n}_e = 2.6 \times 10^{20} m^{-3}$, the recombination region expands along flux surfaces away from the divertor plate towards the x-point and the midplane SOL (Scrape-off Layer) , Fig. 4b, consistent with the

chordal measurements of Fig. 3. This expansion occurs both in the private and common flux regions and corresponds to flux surfaces that impact the outer divertor plate below the 'nose' (see Fig. 1) where the plasma is detached. Finally, in Fig. 4c, the discharge has reached the highest core density, a value of $\bar{n}_e$=3.2x10^{20}m^{-3}. Some recombination is now observed to be inside the separatrix.

There are cases where the core density is increased far past the detachment threshold and a large region of recombination forms INSIDE the separatrix, Fig. 5(a). The density at the time shown, $\bar{n}_e$=3.3x10^{20}m^{-3}, is almost twice the detachment threshold (1.8x10^{20}m^{-3}) for this lower current (0.8 MA), Ohmic discharge. The recombination extends ~4 cm above the x-point. Mapping the recombining region location along flux surfaces to the midplane, its corresponding location there would be ~4.0 mm inside the separatrix. The recombination-dominated character of this 'x-point MARFE (Multifaceted Asymmetric Radiation From the Edge - see a recent review[40] for more references on MARFEs) is very similar to that recently identified for the MARFE at the inner midplane[34]. Similar observations of toroidally-symmetric regions of low-Z impurity dominated radiation moving from the divertor across the separatrix have previously been observed[42-44]. In C-Mod, the low-Z radiating region is further inside the separatrix than the recombination region.

The existence of a cold (< 1eV) and dense (~1.5x10^{20}m^{-3}) recombining region inside the separatrix leads to effects on core radiation and the T_e profile. In Fig. 5(b) the time behavior of the four VUV resonance lines from different ions/atoms are shown for a viewing chord passing through the upper edge of the x-point MARFE [chord shown in Fig. 5(a)]. The O^{5+} (145 eV ionization energy) line intensity peaks and decreases after 0.7 seconds. The sequential peaking and drop in the emission from ions/atoms with successively lower ionization energies implies that the local T_e drops from ~50 eV to ~1 eV. The plasma above the x-point becomes so cold that D^0 line radiation is a major contributor to the radiation power loss from that region. An ECE (Electron Cyclotron Emission) measurement of T_e 2 cm inside the separatrix at the midplane mirrors this cooling effect, Fig. 5(c), but with higher temperatures associated with further inside the core plasma. These discharges can terminate when, and if, the x-point MARFE moves from the x-point to the inner wall and spreads poloidally. All of this occurs at a density corresponding to ~60% of the Greenwald limit[45].

B. Relative magnitude of recombination and divertor plate ion sinks

The detailed profiles of recombination can be integrated to obtain the total recombination sink (I_R) affecting each divertor plate. We utilize recombination 'flux' profiles (#/m^2/s) from views 'O' and 'T' like that shown in Fig. 3. The plane of integration is assumed to be the vertical surface of the outer divertor plate for view 'O' and a horizontal plane through the x-point for view 'T'.

Toroidal symmetry is assumed. A corresponding spatial integration of probe ion saturation current over the divertor surfaces is used to determine the divertor plate ion sink, I_P. The total ion sink is then:

$$I_S = I_R + I_P \qquad (2)$$

where the integration to obtain I_R does not include recombination inside the separatrix. The divertor *ion source* is equal to I_S if dN_{div}/dt is small compared to it (N_{div} is the total number of ions in the divertor). Simple estimates based on measured densities in the divertor (*e.g.* Fig. 3a) and D_γ emissivity contours (Fig. 4), which are strongly correlated with the local density, indicate that $dN_{div}/dt << I_S$ for the plasmas studied. The outer divertor integrals giving $I_{S,R,P}$ are displayed in Fig. 6(a) for the same Ohmic discharge of Figures 3 and 4. Note that we have limited the ion current integral to regions that detach (below the divertor 'nose') and thus correspond to the concentration of outer divertor recombination. The outer divertor plate current, I_P, starts decreasing at ~0.73 seconds, ultimately dropping to ~25% of its peak level. The local drop in ion current can be larger (≥10 near the separatrix) and is simultaneous with local drops in pressure both of which start at ~0.6 seconds, before the ion current integral over the divertor, I_P, drops . Recombination (I_R) increases before detachment **and** before any clear reduction in I_P. In addition, the I_R increase during the discharge is not equal to the drop in I_P. Thus the total *inferred* ion source, equal to I_S, decreases during detachment. By the end of the shot most ions (~75%) created in the divertor recombine before reaching the divertor plate. If we have underestimated the recombination rate (based on our assumptions of constant opacity throughout the divertor region) then an even larger fraction of ions (~90%) would recombine before reaching the plate.

With the geometric information provided by the CCD images such as in Figures 4 and 5 we can compare the relative magnitude of I_R (**only the recombination occurring outside the separatrix, in the divertor**) and I_P over a number of Ohmic discharges with varying $\bar{n}_e$ for the outer divertor. In Fig. 7 we see that as expected, the plate current peaks, and then falls as $\bar{n}_e$ is increased past the detachment threshold ($\bar{n}_e$=1.7x10^{20}m^{-3} for 0.8 MA, =2.3x10^{20}m^{-3} for 1 MA). The higher plate current and detachment threshold for 1 MA Ohmic plasmas is simply due to the higher power flowing into the SOL and divertor. The story is more complicated for I_R. For reference we include a curve (— —) corresponding to the total recombination rate, including the recombination inside the separatrix, for both the 0.8 and 1 MA cases (essentially the same). I_R (only the recombination outside the separatrix) increases linearly through the detachment threshold until I_P starts to asymptote to a minimum for both 0.8 and 1.0 MA discharges. The 0.8 MA discharges are then characterized by a saturation in the recombination level as the x-point MARFE begins forming ($\bar{n}_e$=2.5x10^{20}m^{-3}), substantial recombination occurs inside the separatrix, and $\bar{n}_e$

is further increased. At the highest densities, $\bar{n}_e \geq 3.5 \times 10^{20} m^{-3}$, the x-point MARFE is just beginning to form in 1 MA discharges and there is no discernible saturation of I_R in that case.

C. Inferred Ion source changes

Based on a 'two-point' model (*e.g.* References 5 and 46) for **attached** plasmas one expects the total ion sink (ion source) to scale as $n_e^2 / P_{SOL}^{3/7}$, where n_e is the density upstream in the SOL and P_{SOL} is the power crossing the separatrix into the SOL. For reference we display the attached ion source scaling in Fig. 6(b) utilizing the line-averaged density, $\bar{n}_e$ (roughly proportional to the upstream density) for this almost constant P_{SOL} shot. The difference between the inferred ion source in detachment and that predicted for attached plasmas indicates that the occurrence of detachment reduces the ion source relative to the attached case. This concept is also known as the 'degree of detachment'[47]. Also shown in this figure is the maximum outer divertor ion source calculated assuming that **all** the power flowing into the outer divertor ionization region [~ $0.5 \bullet P_{SOL}$ - P_{Rad} (outer divertor)] is used for creation of ions from neutrals. No power would be left to flow to the divertor plate. *The inferred ion source appears limited by the power flowing into the ionization region.* The magnitude and time behavior of I_P, I_R and I_S are similar for the inner divertor but smaller in magnitude.

There is a clear correlation between the inferred divertor ion source and the power flowing into the ionization region. To illustrate this relationship we first examine the effect of adding auxiliary heating (ICRF) to a detached discharge, Fig. 8(a-b). This discharge is similar to that shown in Fig. 6(a) up until the time ICRF heating is added (0.9 s.). The ICRF and Ohmic heating powers are of similar magnitude (~1.5 MW). When the ICRF is turned on, the divertor is just approaching a detached divertor equilibrium. The immediate effect of the additional power is for the divertor plasma to reattach over much of the plate. The current to the plate increases to values close to that measured in the 'attached' state. The sum of the divertor and core radiation losses increases by ~0.75 MW indicating that ~0.75 MW of additional power flows from the SOL into the divertor ionization regions. The location of the maximum in the recombination rate in the outer divertor leg moves back close to the plate, but I_R decreases only slightly in magnitude! During this movement the recombination volume decreases while the maximum local recombination increases. Adding power to this detached divertor plasma increased the ion source and the local recombination rate.

There are also cases where the power flowing into the ionization region is decreased. We examine an EDA H-mode discharge where the divertor is not detached through an increase in density (as in the above cases), but rather detachment is brought about by increasing impurity radiative losses through injection of N_2 gas, Fig. 8(c-d). The ICRF heating and H-mode begin at ~0.5 and 0.53 s respectively. The divertor starts to detach, with accompanying ion current

reduction, at ~0.8 sec. following the initiation of the N_2 gas feed. The core plasma and pedestal regions are only slightly affected[48-49]. The drop in ion current to the outer plate is similar in magnitude to the Ohmic cases discussed earlier. However, in this case the recombination sink is very low and decreasing as detachment ensues! This result emphasizes that a recombination sink is not necessary to reduce the ion current to the plates. The reduction of the ion source upstream from the divertor plates is the primary cause. *Both a reduction in ion source and an increase in the recombination sink lead to the observed drop in plate current.*

The lack of recombination in these detached H-mode discharges has further implications. Simple estimates (*e.g.* Ref. 50) show that recombination does not play an important role as a momentum sink. This has been verified by experimentally-derived estimates of both the ion-neutral collision and recombination momentum sinks in the same discharge[50-51], at least in these types of discharges. Even in Ohmic discharges, where recombination is at its highest, a calculation of the recombination-related momentum loss leads to pressure decreases that are a fraction (~5%) of that observed. More generally, the quantitative measurements of recombination shown here and elsewhere[50-51], experimentally verify that high levels of recombination are not a necessary condition for divertor detachment.

D. Characteristics of the recombining region

From Fig. 7 we see that as $\bar{n}_e$ and P_{SOL} are varied the amount of recombination in the divertor varies as well. In an effort to understand the scaling of the recombination ion sink we have investigated the characteristics of the recombining region for L-mode plasmas, Fig. 9. The data in this figure are the average of densities obtained through the Stark broadening analysis of Balmer spectra from spectrometer chords passing through the outer [Fig. 9(a)] and inner [Fig. 9(b)] divertor regions. These data are from the same spectra used to infer the recombination rate along each chord. We have performed a linear regression of this data on the variables $\bar{n}_e$ and P_{SOL}, although it is certainly possible that other variables are important. The fit to the data is reasonable in both cases and indicates the strongest dependence on $\bar{n}_e$. We have also looked for any dependence of T_e extracted from the same dataset. T_e varies only slightly and so we find no clear dependence on $\bar{n}_e$ and P_{SOL}, or other variables, to within the experimental error. In the case of H-mode plasmas, the Balmer intensities are too low to extract either n_e or T_e scalings of the recombination region characteristics.

IV. DISCUSSION

A. Power balance

The large range in recombination levels of detached plasmas relative to the total ion sink (10-75%) is striking. This variation implies that the level of recombination is not a determining factor for detachment. However, at the same time recombination can still be a strong sink for ions. The role of recombination as a momentum sink is also under investigation. Such work indicates that, at least in the cases studied so far, recombination does not play an important role in the transfer of momentum from ions to neutrals.

The amount of recombination occurring in the divertor plasma before detachment points towards the possible existence of a dense cold region in the private flux zone prior to moving across the separatrix towards the plates. This region deserves further attention because, as a precursor to detachment on common flux surfaces, it may provide information about how detachment starts and spreads.

The growth of the recombination region as the plasma density is increased past the detachment threshold can have important consequences for the core plasma. The x-point MARFE that forms at the highest densities cools the plasma just inside the separatrix and can lead to a disruption. The fact that this can occur at a fraction of the density limit may lead to insight into the physics of density limit disruptions.

The results presented here show that reduction of ion source can be as important, or more important, in reducing the ion current to the divertor plates than the increase in the recombination sink. We must explain - either with or without a strong recombination sink - how the ion source and sink of particles (I_S) can decrease in detachment. We have already recognized from Fig. 6(b) that, as $\bar{n}_e$ is increased, the inferred ion source increases until a limit, set by power flow into the ionization region, is reached. The ion source is, of course, power limited since ionization converts power into potential energy and photons until little or none is left to be carried to the divertor plates (low T_e and detachment). To aid in understanding this relationship between power and ion source we write several equations describing the power balance in the divertor which hold for all conditions (attached or detached):

$$P_{SOL} = P_{RAD,Z} + P_{RAD,D0} + P_{PLATE}, \quad (3a)$$

$$\text{where } P_{PLATE} = eI_P \, x(\gamma T_e + \varepsilon) \quad (3b)$$

$$\text{and } P_{RAD,D0} \sim eI_S \, x(20 \text{ eV}) + eI_R \, x(10\text{-}12 \text{ eV}) \quad (3c)$$

$P_{RAD,D0}$ and $P_{RAD,Z}$ are the radiated power in the divertor due to D^0 and impurities respectively, ε is the D^0 ionization potential (13.6 eV), γ is the sheath transmission factor (~7), and $I_{P,R,S}$ has

units of #/s. We have assumed that charge-exchange losses are included in P_{RAD}, that $T_i=T_e$, and that 20 eV (10-12 eV) of energy is lost per ionization (recombination) as photons. Momentum loss is, of course, central to detachment and pressure loss, but not explicitly required for this discussion. The first term in the expression for $P_{RAD,D0}$ is the radiation loss from the plasma for each ionization. The second term of Eq. 3(c) is the loss of the ions' potential energy from the plasma through volume recombination as opposed to surface recombination at the plate (eI_P x ε). We collect terms in this equation to achieve a better correspondence to measured quantities and predict I_S (ions/s):

$$I_S = \frac{P_{SOL} - P_{RAD,Z} + e\gamma I_R \langle T_e \rangle}{e(\varepsilon + 20eV + \gamma \langle T_e \rangle)} \tag{4a}$$

$$\langle T_e \rangle \quad \begin{cases} P_{SOL}^{10/7} \quad n_e^{-2} \, [attached], \\ \sim 5 \, eV \; [detached] \end{cases} \tag{4b}$$

$$P_{IONIZ} \quad I_S \, (20 \, eV + \varepsilon) \tag{4c}$$

where n_e is the density upstream in the SOL, $\bar{n}_e$, and P_{IONIZ} is the power expended per ionization in the divertor. The averaging indicated by the '< >' in Eq. 4a is for the flux-weighted average of T_e over the divertor plate. In *attached regimes* $<T_e>$ can be readily predicted by the standard two-point' model (see, for example, References 5 and 46) included in Eq. 4b. For C-Mod *detached regimes* $<T_e>$ is approximately a constant as indicated.

Examining the attached portions of the discharges shown in Figures 6(a) and 8(a), Eq. 4 predicts that increases in $\bar{n}_e$ [constant (P_{SOL}-$P_{RAD,Z}$)] should strongly decrease $<T_e>$ with a resultant strong increase in I_S ($\bar{n}_e^2$). When the divertor becomes detached, Eq. 4 would then predict that I_S would then be independent of $\bar{n}_e$ and dominated by (P_{SOL}-$P_{RAD,Z}$). Thus as (P_{SOL}-$P_{RAD,Z}$) is increased by ~ 0.75 MW [Fig. 8(a)], or decreased by ~ 1.5 MW [Fig. 8(b)], I_S should change proportionately.

We can also examine how well this scaling quantitatively matches the I_S measured. Fig. 10 shows the measured I_S vs. that predicted by Eq. 4a for the detached phase of a number of L-mode discharges. The scaling prediction is similar to the experimental data but consistently higher. The uncertainties in the experimental measurements of P_{SOL} and$P_{RAD,Z}$ cover most of the difference. In addition, it is likely that we are overestimating the power flow from the SOL into the divertor. In the calculation of P_{SOL}, which is based on the difference between the core input power and radiative losses inside the separatrix, we assume that there are no significant perpendicular power

losses in the SOL (i.e. all heat passing through the separatrix is conducted to the divertor region). Recent work[52] indicates that these assumptions are likely violated and that the power flowing into the divertor is lower than the simple estimate described above. Reductions in P_{SOL} by ~ 25% would bring the predicted and measured I_S into agreement for all data points.

B. Characteristics of the recombining region

The data of Fig. 9 indicate that the L-mode recombining region density, $n_{e,r}$, varies widely over the operating range indicated. Since for three-body recombination the recombination rate scales as $S_{recomb} \quad n_{e,r}^3$, the density variation shown in Fig. 9 implies a much stronger variation in recombination rate. The data also show that the density in the recombining region is related to the upstream plasma characteristics. In an effort to understand the derived scaling of Fig. 9, we use the fact that the pressure in the recombining region, $n_r T_r$, is some fraction, δ_r, of the upstream pressure: $(1+M_r^2)n_r T_r = \delta_r n_u T_u$, where the M_r is the Mach number in recombining region. Because $T_r \sim 0.5$ eV, $n_u = \gamma \bar{n}_e$, and $T_u = \eta P_{SOL}^{2/7}$ (conduction-dominated SOL), we can then solve for the recombining region density: $n_r = \delta_r \gamma \eta \cdot \bar{n}_e \cdot P_{SOL}^{2/7} / [(1+M_r^2) \cdot 0.5 \text{ eV}]$. Using experimental fits for γ and η respectively ($\gamma \sim 0.74 \pm 0.11$, $\eta \sim 1.2 \pm .02$), the scalings of Fig. 9 lead to $\delta_r \sim 0.3 \cdot [(1+M_r^2) \cdot \bar{n}_e^{-0.2}]$ where $\bar{n}_e$ is in units of $10^{20} m^{-3}$. Assuming that M_r does not vary significantly, or is small, the terms inside the brackets '[]' are of order 1. The implication is that δ_r is relatively constant at ~ 0.3. We note that at the plate the pressure can be much lower: δ_{plate} is usually in the range 0.01 - 0.1. These results are in qualitative agreement with previous modeling of C-Mod[11] and DIII-D[53] detached plasmas. In Fig. 11 we show the C-Mod modeling results for profiles of density, pressure, recombination and charge-exchange rates along a flux surface up to the divertor plate. The pressure at the plate is not as low a fraction of the upstream pressure as that seen in experiment. Even so, the recombination region, indicated by the peak in the density and recombination rates, occurs at $\delta_r \sim 0.4$ and $M_r \sim 0.1$ (not shown). These modeling results also indicate that i-n collisions, rather than recombination, are the dominant pressure loss mechanism. In the current experimental study, this is also found to be true.

6. SUMMARY

Utilizing measurements of n_e and T_e along the same viewing chords as Balmer series line emission, we are able to determine the local recombination rate as a function of position in the divertor. We find that the recombination region expands from the divertor plate towards the x-point, roughly along flux surfaces, as $\bar{n}_e$ increases and detachment deepens. Comparing the total volumetric recombination ion sink to the plate ion current remaining during detachment, we find that volume recombination eliminates between 10% and 75% of the ion flow before it reaches the

divertor plate. The lowest values are for H-mode plasmas where the detachment is induced by injection of N_2 gas and the power flow into the ionization region is decreased. Recombination is most important as an ion sink for C-Mod discharges when detachment is induced through D_2 gas puffing with the accompanying core density rise. The remaining fraction of the observed ion current reduction is inferred to be due to reductions in the ion source rate upstream from the plate. The inferred ion source rate is consistent with a model relating changes in the divertor ion source to changes in the power flowing into the divertor region.

A scaling for the density in the recombining region is found, $n_{e,r} \quad \bar{n}_e^{0.8} \bullet P_{SOL}^{2/7}$. An implication of this scaling is that the recombining region is found at an approximately constant location along the pressure gradient in the detached region.

Volume recombination can be very important in determining the reduction of ion current to the plates during detachment. Changes in the upstream ion source rate brought about by changes in power flow are equally important. These results also indicate that volume recombination is not a necessary condition for detachment (for either ion current reduction or pressure loss).

ACKNOWLEDGMENTS

The authors wish to thank the entire Alcator group for assistance in acquiring these data. In-depth discussions of the models of detachment with Prof. P.C. Stangeby and Dr. G.M. McCracken were invaluable. This work was supported by the U.S. Dept. of Energy under contract #DE-AC02-78ET51013.

REFERENCES

[1]B. Lipschultz, J. Goetz, B. LaBombard et al., J. Nucl. Mater. **220-222**, 50 (1995).

[2]S. Allen and the DIII-D Team, Plasma Phys. and Control. Fusion **37**, A191 (1995).

[3]J. Neuhauser *et al.*, ibid., A37.

[4]G.F. Matthews, J. Nucl. Mater **220-222**, 104 (1995).

[5]C.S. Pitcher and P.C. Stangeby, Plasma Phys. and Control. Fusion **39**, 779 (1997).

[6]P.C. Stangeby, Nucl. Fusion **33**, 1695 (1993).

[7]K. Borrass & P.C. Stangeby, *Proceedings of the 20th EPS Conference on Controlled Fusion and Plasma Physics, Lisboa, Portugal,* 1993 (European Physical Society, Petit-Lancy, 1993) Vol. 17C, Part II, p. 763.

[8]B. LaBombard, J.A. Goetz, C. Kurz, *et al.*, Phys. Plasmas **2**, 2242 (1995).

[9]S.L. Allen, T.N. Carlstrom, D.G. Wilson, *et al.*, J. Nucl. Mater. **241-243**, 595 (1997).

[10]G.D. Porter, S.L. Allen, M. Brown, *et al.*, Phys. Plasmas **3**, 1967 (1996).

[11]F. Wising, D.A. Knoll, S.I. Krasheninnikov, T.D. Rognlien, and D.J. Sigmar, Contrib. Plasma Phys. **36**, 136 (1996).

[12]A. Loarte, J. Nucl. Mater. **241-243**, 118 (1997) .

[13]K. Borrass, D. Coster, D. Reiter, and R. Schneider, J. Nucl. Mater. **241-243**, 250 (1997).

[14]S.I. Krasheninnikov, A.Yu. Pigarov, D.A. Knoll *et al.*, Phys. Plasmas **4**, 1638 (1997).

[15]D. Lumma, J.L. Terry and B. Lipschultz, ibid. 2555.

[16]R. Isler, G.R. McKee, N.H. Brooks, W.P. West, M.E. Fenstermacher, and R.W. Wood, ibid., 2989.

[17]J.L. Terry, B. Lipschultz, B. LaBombard, D.A. Pappas, *Proceedings of the 24th EPS Conference on Controlled Fusion and Plasma Physics, Berchtesgarten, Germany,* 1997 (European Physical Society, Petit-Lancy, 1997), Vol.21A, P2.022.

[18]B. Napiontek et al., ibid., P4.008.

[19]J.L. Terry, B. Lipschultz, A. Yu. Pigarov, *et al.*, Phys. Plasmas **5**, 1759 (1998).

[20]G.M. McCracken, M.F. Stamp, R.D. Monk, A. Meigs, J. Lingertat, R. Prentice, A. Starling, and R. Smith, Nucl. Fusion **5**, 619 (1998).

[21]J.L. Terry, B. Lipschultz, X. Bonnin, *et al.*, 'Volume recombination and opacity in Alcator C-Mod plasmas', *13th Conf. on Plasma Surface Interactions in Controlled Fusion,* 18-22 May, 1998, San Diego, Ca., paper I-1, accepted to J. Nucl. Mater.

[22]B. Lipschultz, J.L. Terry, C. Boswell, S.I. Krasheninnikov, B. LaBombard, and D.A. Pappas, 'Recombination and ion loss in Alcator C-Mod detached divertor discharges', ibid., paper O-28, accepted to J. Nucl. Mater.

[23]G.M. McCracken, L. Horton, J. Lingertat, G.F. Matthews, A. Meigs, R.D. Monk, M.F. Stamp, and P.C. Stangeby, 'Volume recombination in JET divertor plasmas', ibid., paper I-2, accepted to J. Nucl. Mater.

[24]U. Wenzel, K. Behringer, A. Carlson, *et al*., ibid. paper 3P-51, and *Proceedings of the 25th EPS Conference on Controlled Fusion and Plasma Physics, Prague, Czech Republic,* 1998 (European Physical Society, Petit-Lancy, 1998), Paper P2.010.

[25]G.S. Chiu and S.A. Cohen, Phys. Rev. Lett. **76**, 1248 (1996).

[26]N. Ezumi, N. Ohno, Y. Uesugi, J. Park, S. Watanabe, S.A. Cohen, S.I. Krasheninnikov, A.Yu. Pigarov, M. Takagi, and S. Takamura. *Proceedings of the 24th EPS Conference on Controlled Fusion and Plasma Physics, Berchtesgarten, Germany,* 1997 (European Physical Society, Petit-Lancy, 1997), Vol.21A, p. 1225.

[27]I.H. Hutchinson, R. Boivin, F. Bombarda, *et al*., Phys. Plasmas **1**, 1511 (1994).

[28]Y. Takase, R. Boivin, F. Bombarda, et al., *Proceedings of the 16th International Fusion Energy Conference, Montreal,* 1996 (International Atomic Energy Agency, Vienna, 1997), Vol. 1, p. 475.

[29]A.E. Hubbard, R.L. Boivin, R.S. Granetz, *et al*., Phys. Plasmas **5**, 1744 (1998).

[30]A. Allen, Ph.D. thesis, Massachusetts Institute of Technology, Cambridge, Ma. MIT Plasma Science & Fusion Center report PSFC/RR-97-1, Feb. 1997.

[31]R.K. Janev, D.E. Post, W.D. Langer, K. Evans, D.B. Heifitz, and J.C. Weisheit, J. Nucl. Mater. **121-122**, 10 (1984).

[33]D.E. Post, J. Nucl. Mater. **220-222**, 143 (1995).

[33]S.I. Krasheninnikov, A.Yu. Pigarov, and D.J. Sigmar, Phys. Lett. **214**, 285 (1996).

[34]A.Yu. Pigarov and S.I. Krasheninnikov, Phys. Lett. A. **222**, 251 (1996).

[35]R. Bengston, J.D. Tannich and P. Kepple, Phys. Rev. A **1**, 532 (1970).

[36]J.L. Terry, B. Lipschultz, C.J. Boswell, B. LaBombard, D.A. Pappas, A.Yu. Pigarov, Bull. Amer. Phys. Soc. **43**, 1708 (1998).

[37]D. Post, J. Nucl. Mater. **220-222**, 143 (1995).

[38]D. Lumma, "Investigation of a diagnostic technique for measuring electron densities via Stark broadening on the Alcator C-Mod tokamak", M.S. thesis, M.I.T. 1996.

[39]M.E. Fenstermacher, S.L. Allen, T.E. Evans, *et al*., 'Evolution of 2D deuterium and impurity radiation profiles during transitions from attached to detached divertor operation in DIII-D,' *13th Conf. on Plasma Surface Interactions in Controlled Fusion*, 18-22 May, 1998, San Diego, Ca., paper O-23, accepted to J. Nucl. Mater.

[40]B. Meerson, Rev. Mod. Phys. **68**, 215 (1996).

[41] B. Lipschultz, J.L. Terry, C. Boswell, A.E. Hubbard, B. LaBombard, and D.A. Pappas, Phys. Rev. Lett. **81**, 1007 (1998).

[42] N. Hosogane, K. Itami, N. Asakura, H. Kubo, K. Shimizu, S. Tsuji, M. Shimada, J. Nucl. Mater. **220-222**, 420 (1995).

[43] J.A. Goetz, C. Kurz, B. LaBombard, Phys. Plasmas **3**, 1908 (1996).

[44] T.W. Petrie, S.L. Allen, T.N. Carlstrom, *et al*., J. Nucl. Fus. **241-243**, 639 (1997).

[45] M. Greenwald, J.L. Terry, S.M. Wolfe, S. Ejima, M. Bell, S. Kaye, G.H. Nielson, Nucl. Fusion **28**, 2199 (1988).

[46] P. Stangeby, in *The Plasma Boundary of Magnetic Fusion Devices* to be published by the Institute of Physics Publishing, Techno House, Redcliffe Way, Bristol BS1 6NX, U.K.

[47] A. Loarte, R.D. Monk, J.R. Martin-Solas, Nucl. Fus. **38**, 331(1998).

[48] J.A. Goetz, B. LaBombard, B. Lipschultz, *et al*., "High confinement dissipative divertor operation on Alcator C-Mod", submitted to Phys. Plasmas (this conference).

[49] A.E. Hubbard, R.L. Boivin, J.A. Goetz, M. Greenwald, B. Lipschultz, Bull. Amer. Phys. Soc. **43**, 1706 (1998).

[50] C.S. Pitcher, B. LaBombard, B. Lipschultz, J. Weaver, B. Welch, 'The roles of friction and recombination in SOL pressure balance', *13th Conf. on Plasma Surface Interactions in Controlled Fusion*, 18-22 May, 1998, San Diego, Ca., paper 2P-67, accepted to J. Nucl. Mater.

[51] B. Lipschultz, C. Boswell, J.A. Goetz *et al*., *17th IAEA Fusion Energy Conference*, 19-24 November, 1998, Yokohama Japan., paper F1-CN-69/EX3/3.

[52] M. Umansky, S.I. Krasheninnikov, B. LaBombard, and J.L. Terry, Phys. Plasmas **5**, 3373 (1998).

[53] M.E. Fenstermacher, S.L. Allen, N.H. Brooks, *et al*., Phys. Plasmas **4**, 1761 (1997).

FIGURE CAPTIONS

Figure 1: The Alcator C-Mod divertor region. The separatrix is shown as a dashed line. View 'O' includes 7 chordal views of the outer divertor. View 'T' includes chordal views of both divertor regions. Viewing chords have < 1 cm spatial resolution.

Figure 2: Typical D^0 recombining spectra in the VUV (a) and visible (b). Dashed line in (a) represents a radiative recombination model with emission region length = 1.5 cm, n_e=1.8x10^{21} m^{-3}, T_e=0.7 eV. (c) A Voigt fit to the $8 \rightarrow 2$ Balmer line to obtain Stark width and n_e. (d) Fit of Saha distribution to D^0 population densities to obtain T_e.

Figure 3: Evolution of the outer divertor characteristics. (a) n_e profiles derived from Stark broadening of Balmer $8 \rightarrow 2$ line; (b) T_e derived from fit of Saha distribution to Balmer population densities ($5 \rightarrow 8$); (c) Local recombination rate based on n_e, T_e, Dγ intensity, assumptions of opacity, and recombinations/photon factor[19].

Figure 4: Dγ emissivity contour plots obtained by inversion of CCD images for 3 times (a) 0.6 sec., $\bar{n}_e$=2.3x10^{20} m^{-3} shortly after the start of detachment; (b) 0.8 sec., $\bar{n}_e$=2.6x10^{20} m^{-3}; and (c) 1.0 sec., $\bar{n}_e$=3.2x10^{20} m^{-3}. Maximum contour 7.7kW/m^2. Each contour step 0.96 kW/m^2.

Figure 5: Recombination occurring inside the separatrix shown by Dγ emission and analysis of n_e and T_e from that region: (a) Dγ emissivity contour plots obtained by inversion of CCD image at 1.0 seconds. Maximum contour 5kW/m^2. Each contour step 0.62 kW/m^2. (b) VUV brightnesses from a horizontal chord through the upper edge of the recombination region (Fig. 5a) above the x-point; all normalized to the same level. (c) T_e, 2 cm inside the separatrix on the midplane, determined from ECE emission measurements.

Figure 6: (a) Ion sinks for the outer divertor plate in 1MA Ohmic detachment (starts at ~0.75 sec.) where $\bar{n}_e$ is increased continuously until 1.0 seconds; $I_{Sink}=I_{Plate}+I_{Recomb}$. (b) Comparison of the inferred outer divertor ion source to $\bar{n}_e^2$ (scaled to match I_{Sink} at 0.4 seconds) and the net power flowing into the outer divertor ionization region converted to ion flux [$=P_{NET}/(e \cdot 30\ eV)$].

Figure 7: Divertor recombination and plate ion sinks for two different plasma currents vs. $\bar{n}_e$. 0.8MA: I_R (●), I_P (——). 1MA: I_R (❑), I_P(- - - -). Also shown is the total recombination, including that inside the separatrix, for both currents (— —).

Figure 8: ICRF heating of detached plasma (detachment starts at ~0.6 seconds); (a) Ion sinks, (b) line-averaged density; and, detachment of an H-mode plasma with N_2 gas (detachment starts at ~0.7 seconds); (c) Ion sinks, (d) line-averaged density.

Figure 9: Linear regression of recombining region n_e derived from Stark broadening of Balmer $8 \rightarrow 2$ brightnesses averaged over (a) inner and (b) outer divertor regions. Each plotted vs. best linear regression fit to the power flowing into the SOL, P_{SOL}, and $\bar{n}_e$.

Figure 10: Divertor ion source inferred from measured sinks plotted against the divertor ion source predicted by Eq. 4a.

Figure 11: UEDGE modeling of a C-Mod detached divertor discharge[11]. Shown are the pressure, ion density, rates for charge-exchange and recombination along a flux surface near the separatrix leading to the outer divertor plate. Recombination is peaked in the high density region at ~ δ_r=0.4.

Figure 1

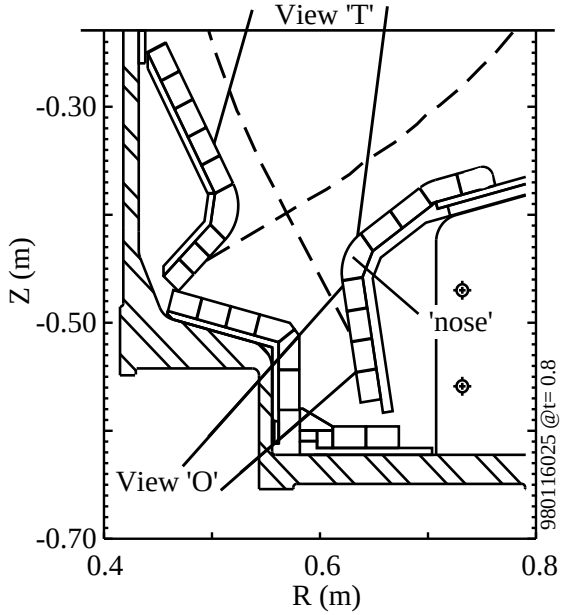

Figure 2

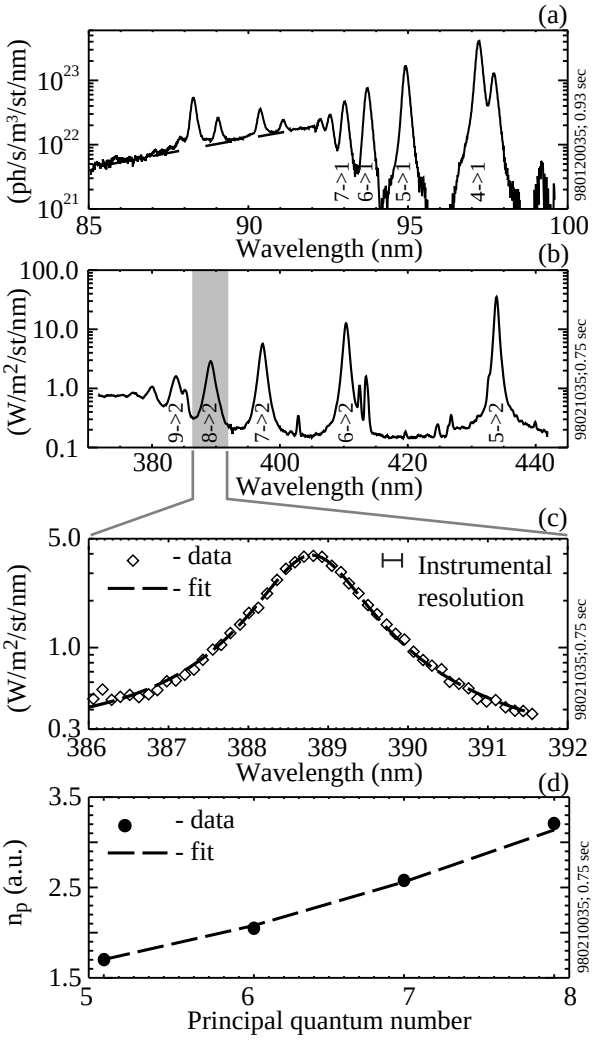

Figure 3

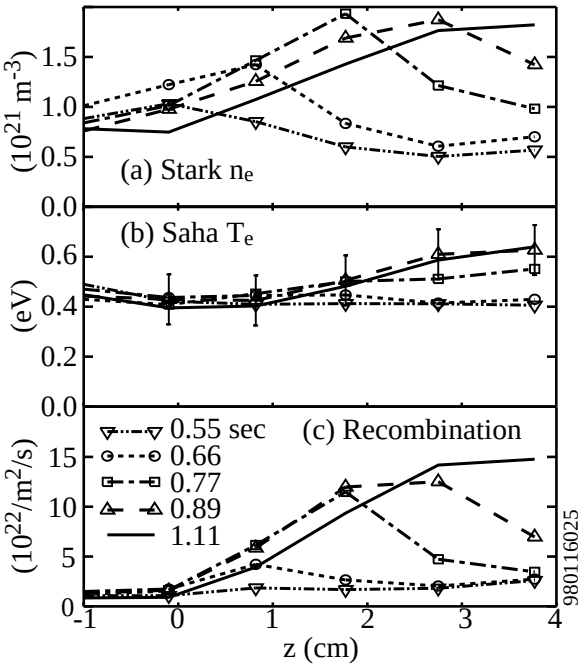

Figure 4

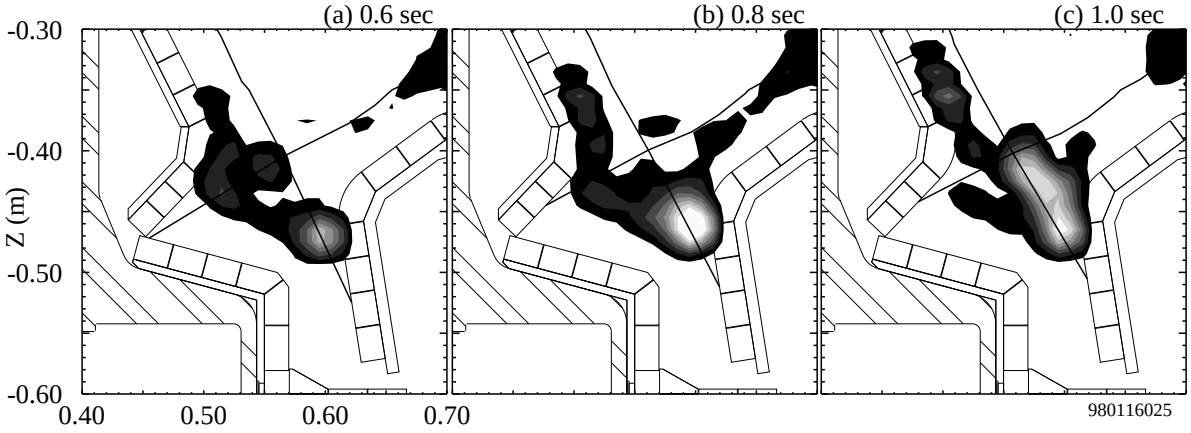

Figure 5

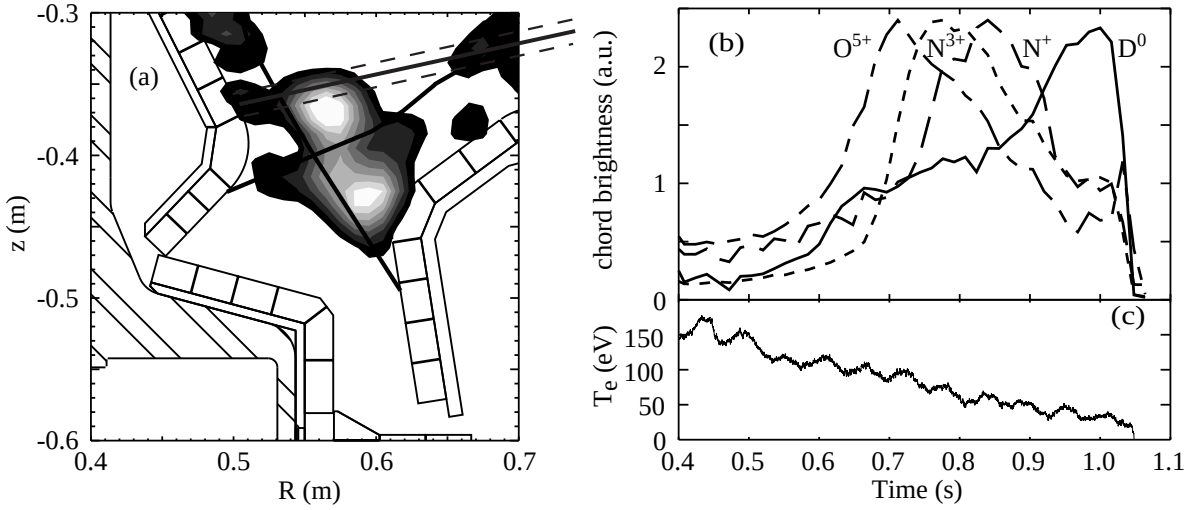

Figure 6

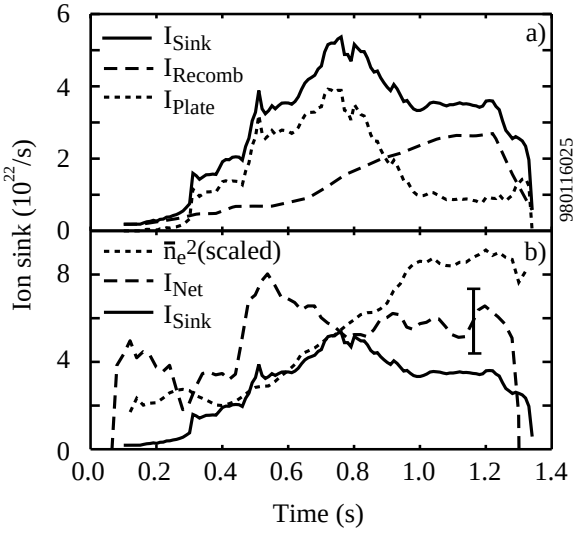

Figure 7

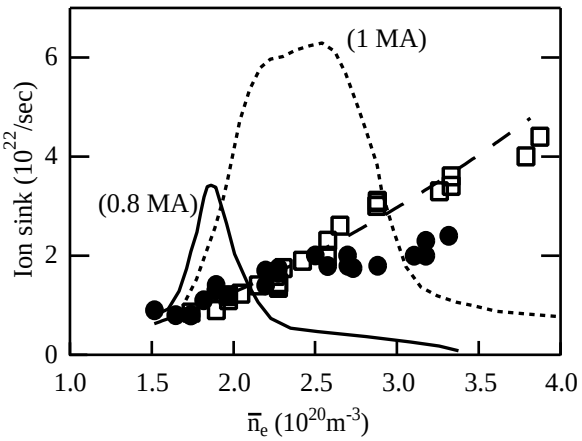

Figure 8

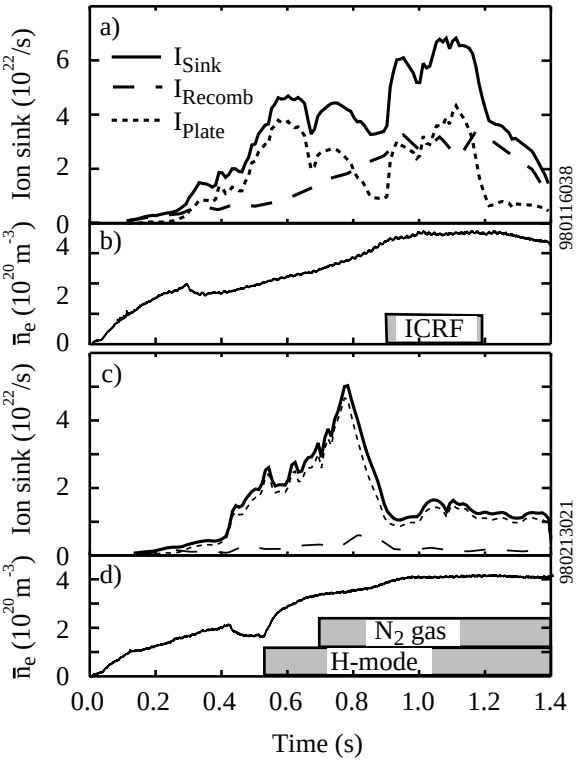

Figure 9

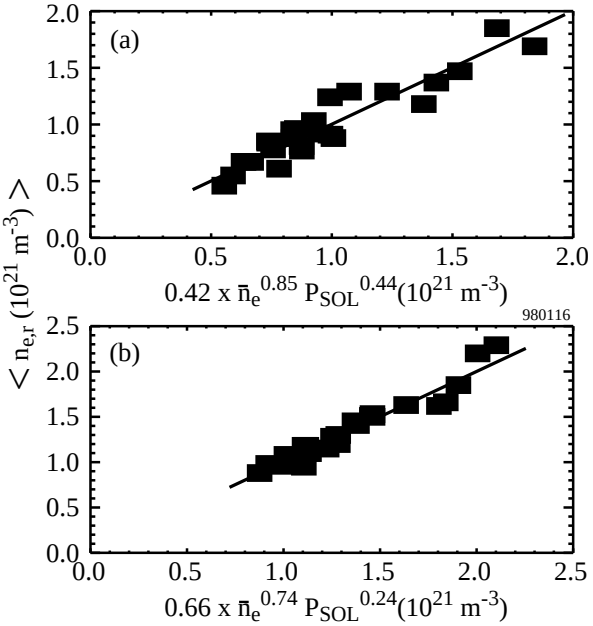

Figure 10

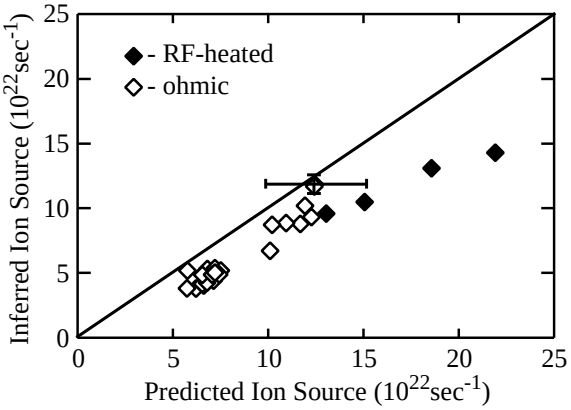

Figure 11